MATERIALE PLASTICE
https://revmaterialeplastice.ro
https://doi.org/10.37358/Mat.Plast.1964

Track Model with Nonlinear Elastic Characteristic of the Rubber Rail Pad

TRAIAN MAZILU[1]*, SORIN ARSENE[1]*, IOAN-CRISTIAN CRUCEANU[2]
[1] University Politehnica of Bucharest, Faculty of Transport, Department of Railway Vehicles, 313 Splaiul Independentei 060042, Bucharest, Romania
[2] University Politehnica of Bucharest, Faculty of Transport, Doctoral School of Transport, 313 Splaiul Independentei, 060042, Bucharest, Romania

Abstract: *This paper presents a new basic nonlinear track model consisting of an infinite Euler-Bernoulli beam (rail) resting on continuous foundation with two elastic layers (rail pad and ballast bed) and intermediate inertial layer (sleepers). The two elastic layers have bilinear elastic characteristic obtained from the load-displacement characteristic of the rail pad and ballast. A time-varying load with two components - time-constant one and harmonic other, representing the wheel/rail contact force is considered as the track model input. Rail deflection due to the time-constant component of the load is obtained solving the nonlinear equations of the balance position. Subsequently, the structure of the nonhomogeneous foundation is determined. Dynamic response of the rail in terms of receptance due to the harmonic component of the load is calculated using the linearised track model with nonhomogeneous elastic characteristic. Influence of the time-constant component and the reflected waves due to the nonhomogeneous foundation are presented.*

Keywords*: track, rubber rail pad, nonlinear characteristic, bilinear function, rail receptance*

1. Introduction

Track modelling is crucial for the study of the interaction between the trains and track. This research topic has many technical applications because the railway traffic is developing unwanted vibration and noise which affect the track superstructure, the rolling stock, the passenger comfort, and the life conditions in the track area.

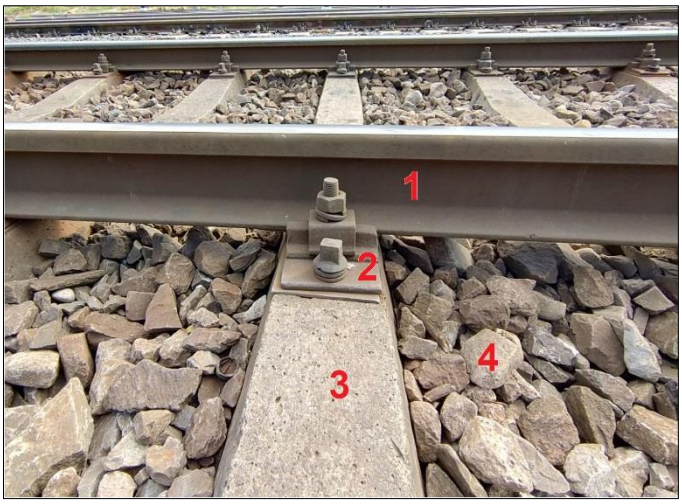

Figure 1. Ballasted track: 1. Rail, 2. fastening system, 3. concrete sleeper, 4. ballast bed

Traditional track consists of two rails laid via rail pad and fastening system on concrete/wooden sleepers which are arranged at regular distances from each other on the ballast bed (Figure 1).

**email: traian.mazilu@upb.ro, sorin.arsene@upb.ro*

For the track modelling the most used methods are the analytical method, mode-superposition method, boundary element method, finite element method, and discrete element method. Analytical methods use two kinds of models for the rail, the Euler-Bernoulli beam [1] and Timoshenko beam model [2]. These methods allow to consider the track model of infinite length which is very convenient because the effect of the reflected waves by the model edges is removed. The mode-superposition method is an efficient tool to perform the time-domain analysis of the vehicle/track interaction [3]. Boundary element method is preferred when the rolling noise problem is investigated [4]. The finite element method is recommended to model the track at high frequency due to the possibilities of modelling the constructive details of the track, but this advantage comes with a cost in terms of time consuming and computer capacity [5]. The discrete element method allows to simulate the sophisticated dynamic behaviour of the stone components of the ballast bed [6].

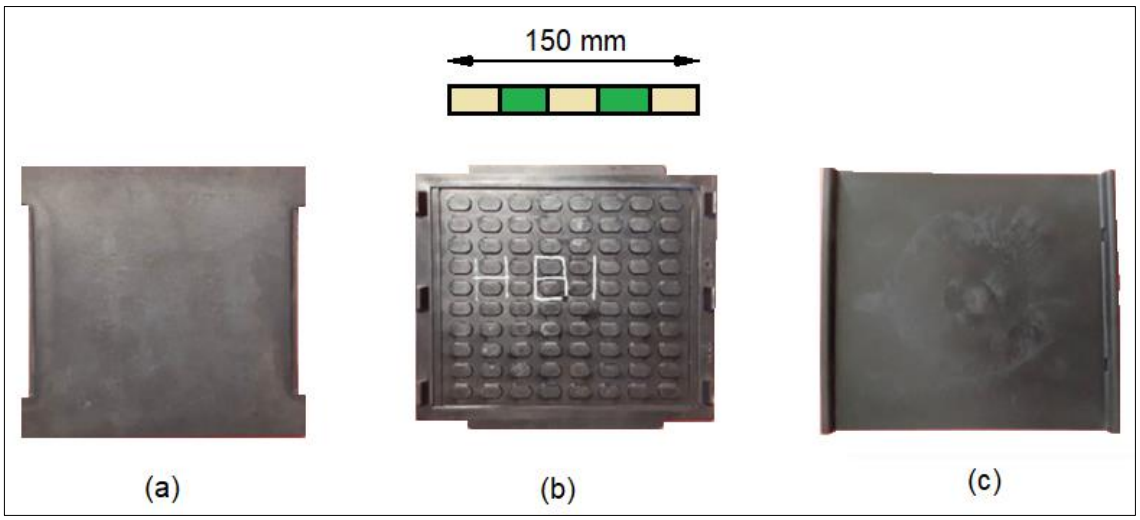

Figure 2. Rail pad varieties: (a) of EPDM; (b) of TPE; (c) of EVA, after [8]

The rail pads play an important role in the wheel/rail dynamics because they are the closest elastic elements to the wheel/rail contact patch. The rail pads are assembled between the steel rails and sleepers to distribute the wheel/rail load over a large surface avoiding the resultant fatigue and shock stresses. Usually, the rail pads are made of rubber, ethylene propylene diene monomer (EPDM), thermoplastic polyester elastomer (TPE), high-density polyethylene (HDPE), and ethylene-vinyl acetate (EVA), as presented in Figure 2 [7, 8]. Such materials are well known in industry and these are extensively studied from many view points to solve various practical issues [9-14].

From mechanical viewpoint, the rail pad has nonlinear characteristics in both quasistatic behavior (load-deflection curve) and frequency response function as revealed in some research [8, 15-17].

The modelling of fastening systems, including the rail pad modelling has been extensively treated in papers like the references [18-21]. The main representation of the rail pad is the Kelvin-Voigt system which consists in a linear elastic element working in parallel with a viscous damper element [2]. This model can be applied in the analytical representation of the track. When the FEM is used to model the rails and sleepers, the rail pad should be modelled as a line of many discrete Kelvin-Voight systems or even as an area covered by such systems [18, 21]. Other approach regarding the rail pad modelling is represented by the fractional derivative model [20]. The nonlinearity of the elastic characteristic of the rail pad is introduced via polynomial functions [22].

In this paper, a new basic analytical model of the track based on the approximation of the nonlinear elastic characteristic of the rail pad using the bilinear functions is presented. Also, the nonlinear elastic characteristic of the ballast bed [8] is introduced via a bilinear function. Rail pad and ballast damping is considered as hysteretic damping. In short, track model consists of a beam (rail) resting on a continuous foundation with two elastic layers, both with bilinear elastic characteristic. The rail is under a time-

varying load with two components, one is time-constant, representing the static load of a vehicle per wheel, and other one is of harmonic type, corresponding to the dynamic component of the wheel/rail force. Rail response is split in two according to the two components of the time-varying load. Rail deflection due to the time-constant load is calculated using the nonlinear model of the track and then, the rail receptance is derived with the help of the linearized model with nonhomogeneous foundation.

2. Mechanical model of the track

2.1. Modelling of the elastic characteristic of rail rubber pad and ballast

Figure 3 shows the nonlinear elastic characteristic of a rail rubber pad and ballast. Rail rubber pad is part of the K-type rail fastening system [23] and its elastic characteristic consists of the low (elastic) and upper (rigid) limit curves (Figure 3a). Force-deformation diagram of a particular rail rubber pad must be situated between the two limit curves to be proper for using. The mean elastic characteristic is also shown in Figure 3a, and this is taken as reference in the followings. When mounted on the track, the rail rubber pad is prestressed by 10 kN, and the deformation of 0 mm in the figure corresponds to the prestressed condition.

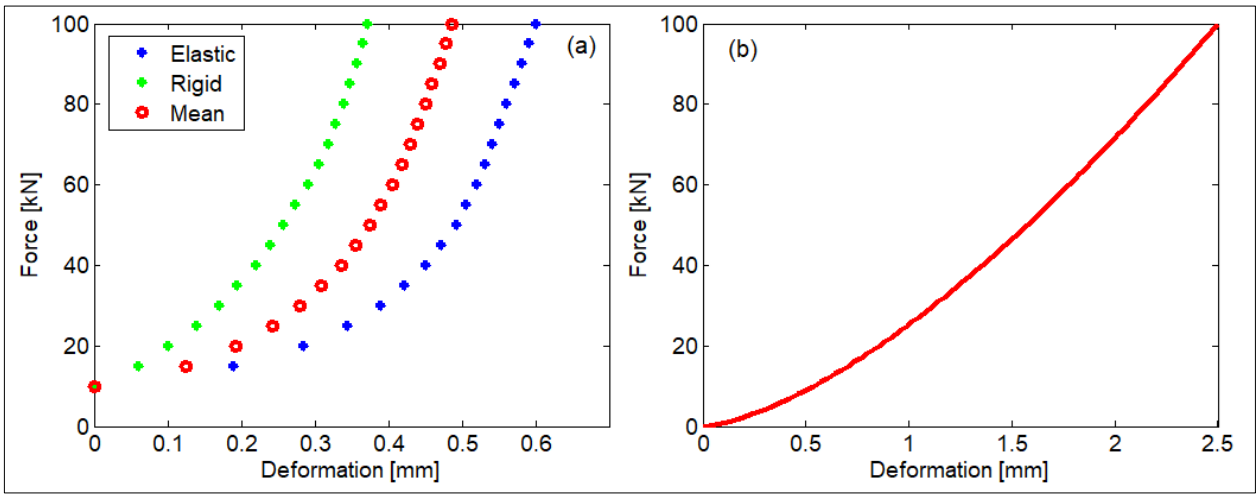

Figure 3. Elastic characteristic of the rail rubber pad and ballast: (a) Limit and mean curves of the elastic characteristic of the rail rubber pad for the K-type rail fastening system (after [23]); (b) ballast (after [15])

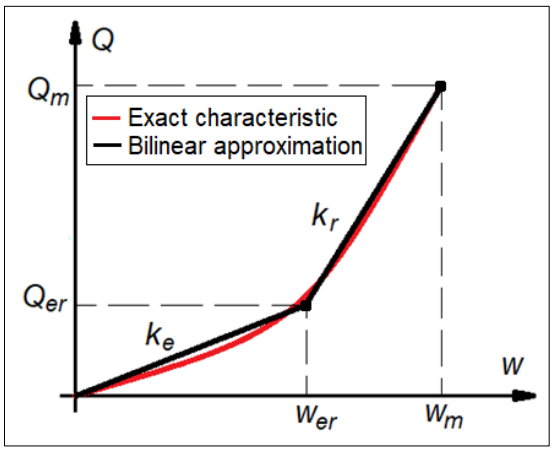

Figure 4. Bilinear approximation

Elastic characteristic of the ballast corresponds to a semi-sleeper and it is designed according to the

following Hertzian formula recommended by Wu and Thomson [15].

$$Q = C_H \delta^{3/2} \tag{1}$$

where Q is the force, d – the deformation and C_H – the Hertzian constant; C_H = 800 MN/m$^{3/2}$.

These elastic characteristics could be included into the track model in a simplified form as two piecewise linear functions (bilinear approximation (Figure 4)).

$$Q(w) = \begin{cases} k_e w & 0 \le w < w_{er} \\ Q_{er} + k_r (w - w_{er}) & w_{er} \le w \le w_m, \end{cases} \tag{2}$$

where k_e and k_r are the 'elastic' and 'rigid' elastic constants of the bilinear characteristic, (w_{er}, Q_{er} = $k_e w_{er}$) are the coordinates of the transition point from elastic to rigid portion of the bilinear characteristic, and (w_m, $Q_m = Q_{er} + k_r(w_m - w_{er})$) are the coordinates of the limit point of the bilinear characteristic.

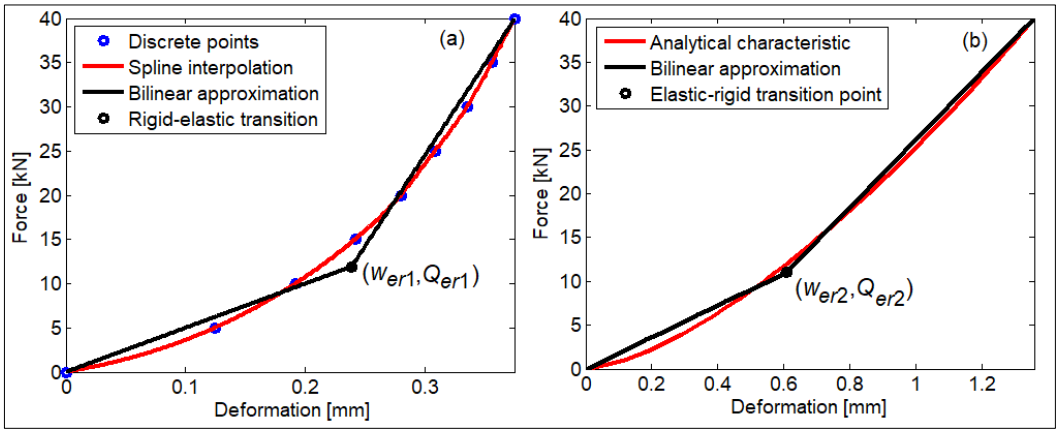

Figure. 5. Bilinear approximation of the elastic characteristic of the rail rubber pad and ballast: (a)rail rubber pad; (b) ballast

Construction of the bilinear characteristic may be obtained using the least square method, which means that the sum of the squared residuals must be minimised. The residual is the difference between the value of the exact characteristic, and the value of the bilinear approximation.

Results of the applying of the least square method is displayed in Figure 5, where the exact characteristics of the rail rubber pad and ballast and their bilinear approximations can be traced for the static load of 40 kN. Starting from the discrete points of the rail rubber pad elastic characteristic, many other points have been obtained by spline interpolation and then, the bilinear approximation has been calculated (Figure 5a). The elastic characteristic of the ballast has analytical shape (Eq. 1) and this form has been used to obtain the bilinear approximation (Figure 5b). The elastic constants of the bilinear characteristic of the rail rubber pad are k_{e1} = 49.87 kN/mm for the elastic portion and k_{r1} = 205.56 kN/mm for the rigid portion; the transition point has the coordinates of w_{er1} = 0.239 mm and Q_{er1} = 11.92 kN. The elastic constants of the bilinear characteristic of the ballast are k_{e2} =17.19 kN/mm for the elastic portion and k_{r2} =39.34 kN/mm for the rigid portion; the coordinates of the transition point are w_{er2} = 0.605 mm and Q_{er2} = 10.40 kN.

Errors introduced by the bilinear approximation does not exceed 6.9% for the rail rubber pad and 3.75% for the ballast. The RMS value of the errors is less than 3.0% for the rail rubber pad and 1.7 % for the ballast.

2.1.2. Track model

In this section, the track model depicted in Figure 6 is considered. The model is based on the symmetry property of the track with respect to the longitudinal axis, and due to that, only half of its structure is modelled. Influence of the spacing of the sleepers is neglected and, therefore, the model of

the track is reduced to a beam on a continuous foundation with two elastic layers. The first elastic layer under the beam shapes the elasticity of the rail pads, while the second elastic layer shapes the ballast.

The rail is assimilated with an infinite Euler-Bernoulli beam having constant section and whose linear mass is equal to the mass of the rail per unit length. The beam has the bending stiffness given by the moment of inertia of the cross section, I, and by the longitudinal modulus of elasticity of the material from which the rail is made, E. The internal friction in rail is neglected.

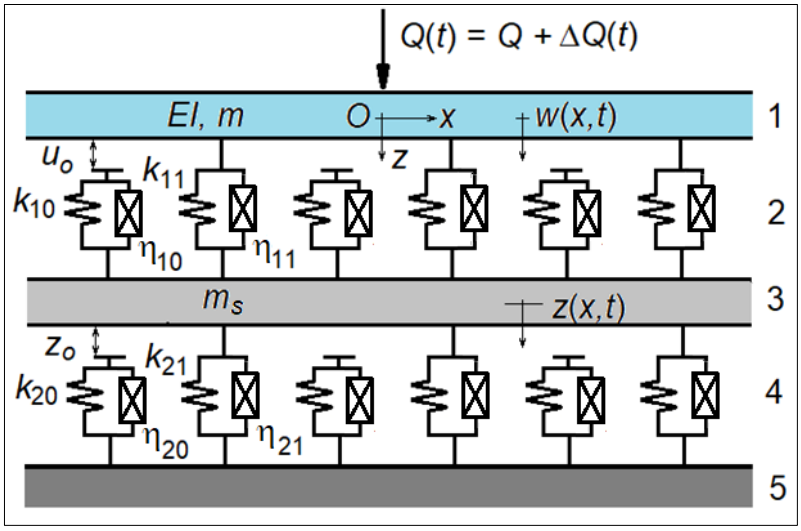

Figure 6. Track model: 1. Euler-Bernoulli beam - rail; 2. Winkler foundation with bilinear characteristic - rail rubber pad; 3. Inertial layer - sleepers; 4. Winkler foundation with bilinear characteristic - ballast; 5. Rigid base

The model of the rail pads is represented by Winkler foundation with bilinear characteristic and hysteretic damping. The elastic constants are k_{11} and k_{10}, and the loss factors are η_{11} and η_{10}. The stiffness jump occurs when the relative displacement between the rail and the sleepers is $u_o = w_{er1}$ and the elastic constant of the rail pad becomes $k_{12} = k_{11} + k_{10}$. Corresponding, the loss factor takes the value of $\eta_{12} = (k_{11}\,\eta_{11} + k_{10}\,\eta_{10})/k_{12}$.

The elastic and damping characteristics of the ballast are shaped similarly to the case of the rail pads. The elastic constants are k_{21} and k_{20}, and the loss factors are h_{21} and h_{20} for ballast. The jump of stiffness occurs when the sleeper displacement is $z_o = w_{er2}$ and the elastic constant of the ballast is $k_{22} = k_{21} + k_{20}$ and, the corresponding loss factor is $\eta_{22} = (k_{21}\,\eta_{21} + k_{20}\,\eta_{20})/k_{22}$.

The values of the elastic constants k_{ij} with $i, j = 1, 2$ result from the above calculated stiffnesses of the rail pad and ballast divided to the sleeper bay, d,

$$\begin{aligned} k_{11,12} &= k_{e1,r1}/d \\ k_{21,22} &= k_{e2,r2}/d \end{aligned} \tag{3}$$

The elastic constants k_{10} and k_{20} are introduced due to the coherence reason of the track model. Knowing the $k_{11,12}$ and $k_{21,22}$ elastic constants given by Eq 3, the values of the k_{10} and k_{20} elastic constants result.

The bilinear characteristic of each elastic layer can be designed in terms of the uniform load [N/m] versus displacement (Figure 7). Transition points of coordinates (u_o, q_{10}) for the rail pad and (z_o, q_{20}) are related by

$$\begin{aligned} q_{10} &= k_{11}u_o \\ q_{20} &= k_{21}z_o \end{aligned} \tag{4}$$

Next, corresponding to the results above, it considers that $q_{10} > q_{20}$.

According to this type of the track model, the sleepers are represented by an inertial layer that takes neither shear force nor bending moment. The mass per unit length of the inertial layer is calculated with the relation

$$m_s = \frac{M_s}{2d}, \tag{5}$$

where M_s is the sleeper mass and d is the sleeper bay.

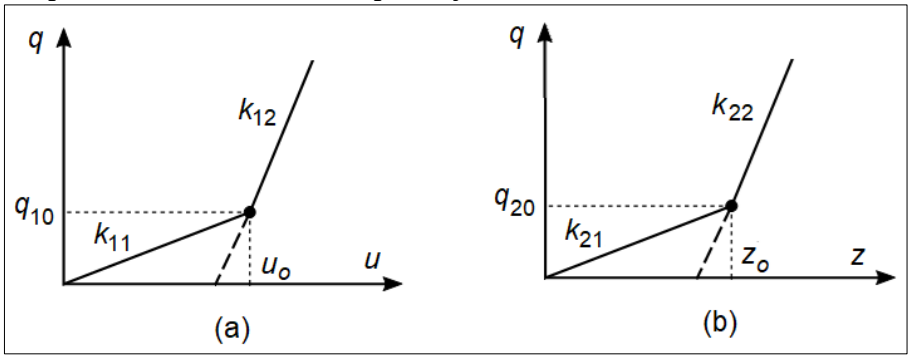

Figure 7. Bilinear characteristic of the elastic layers: (a) rail pad; (b) ballast

A force, $Q(t)$, acts on the rail, which has a constant component, Q, corresponding to the static load of the vehicle on a wheel and a harmonic component of amplitude much smaller than the magnitude of the static load and given frequency, $\Delta Q(t)$. The latter component corresponds to the dynamic wheel-rail contact force. It holds

$$Q(t) = Q + \Delta Q(t). \tag{6}$$

As the speed of trains is much slower than the speed of the propagation of the elastic waves through the track, the effect induced by the displacement of the force is neglected and, therefore, it assumes that the force has fixed support.

The origin of the reference system, Oxz, against which the movement of the beam and the inertial layer (of the sleepers) is studied, is in the neutral axis of the beam. The reference position is the position of the beam and the inertial layer under its own weight on the elastic foundation.

In a section x, the displacement of the beam is $w(x, t)$, and that of the inertial layer, $z(x, t)$. For simplicity, it is considered that the force acting on the beam has the support in the section of the origin of the reference system.

Given that the force $Q(t)$ has two components, one static and the other dynamic, and the response of the beam and the inertial layer will have two components accordingly

$$\begin{aligned} w(x,t) &= w(x) + \Delta w(x,t) \\ z(x,t) &= z(x) + \Delta z(x,t). \end{aligned} \tag{7}$$

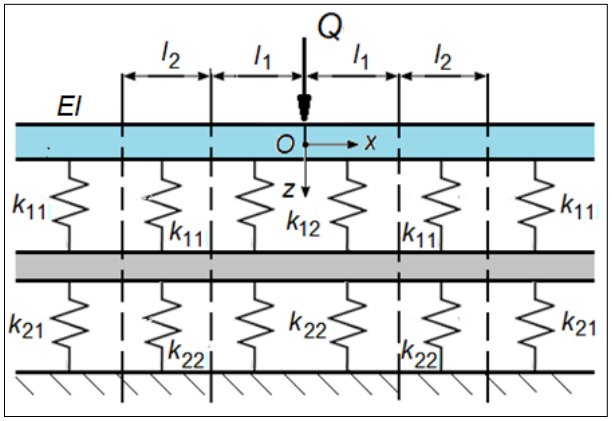

Figure 8. Track under static load

The static components $w(x)$ and $z(x)$ can be calculated considering that only the static component of the force, Q, acts on the beam, while the dynamic components, $\Delta w(x, t)$ and $\Delta z(x, t)$, result as an effect of the motion of the system under the action of the dynamic component of the force, $\Delta Q(t)$.

To find the balance position of the track under the static load Q, the nonlinear model of the track is used. Depending on the magnitude of the static load, three cases can be exposed: for small static load, the rail pad and ballast work on the elastic portion of their bilinear characteristics.

For medium values of the static load, the ballast works around the static load section on the rigid portion of the bilinear characteristic and on the elastic portion in rest; the rail pad works only on the elastic portion.

For high values of the static load (Figure 8), there is a region around the static load section of $2l_1$ length, where both rail pad and ballast work on the rigid portion of their bilinear characteristics. Beyond this region, there is other region of l_2 length, where the ballast works on the rigid portion of its bilinear characteristic, meanwhile the rail pad works on the elastic portion. Further on, there is other region, the third, which expands to infinite, where both rail pad and ballast work on the elastic portion of the bilinear characteristics. Obviously, the track structure has the loading section as the centre of symmetry.

Next, the solution of the third case is shown because the fact that this case is usual. To this aim, the boundary condition method is applied.

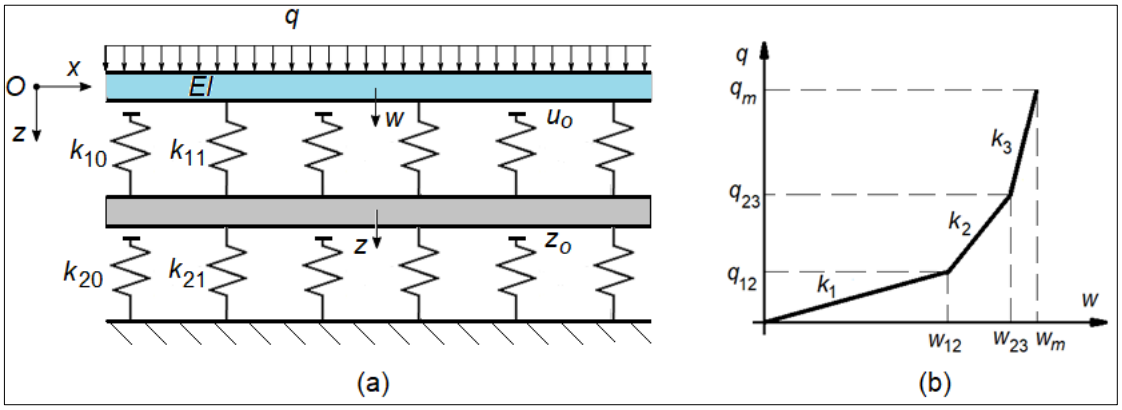

Figure. 9. Explanatory for the determination of the equivalent elastic characteristic: (a) track loading; (b) equivalent elastic characteristic

First, the equivalent elastic characteristic of the track model is built up (Figure 9). This characteristic shows the evenly distributed load acting on the rail depending on its displacement. There are three branches with the stiffnesses k_1, k_2 and k_3 and two transition points of coordinates (w_{12}, q_{12}) and (w_{23}, q_{23}). First point corresponds to the point of transition in the ballast characteristic, and the second one corresponds to point of transition in the rail pad characteristic. It holds

$$k_1 = \frac{k_{11}k_{21}}{k_{11}+k_{21}}, \quad k_2 = \frac{k_{11}k_{22}}{k_{11}+k_{22}}, \quad k_3 = \frac{k_{12}k_{22}}{k_{12}+k_{22}}, \qquad (8)$$
$$q_{12} = q_{20}, \quad q_{23} = q_{10}.$$

The rail and sleeper displacement for the two transition points can be calculated using the equations

$$w_{12} = z_o\left(1+\frac{k_{21}}{k_{11}}\right), \quad w_{23} = u_o\left(1+\frac{k_{11}}{k_{22}}\right)+z_o\left(1-\frac{k_{21}}{k_{22}}\right),$$
$$z_{12} = z_o, \quad z_{23} = u_o\frac{k_{11}}{k_{22}}+z_o\left(1-\frac{k_{21}}{k_{22}}\right). \qquad (9)$$

In the following, only half of the track model is considered due to the symmetry (Figure 10). Inserting

the $O_ix_iz_i$ reference systems and the rail displacements $w_i(x_i)$ with i = 1 – 3, the following equations describe the rail equilibrium under the static load

$$\frac{d^4 w(x_i)}{dx_i^4} + 4\alpha_i^4 w(x_i) = 0 \tag{10}$$

where:

$$0 \le x \le l_1, \quad 0 \le x_2 \le l_2, \quad 0 \le x_3, \quad \alpha_i^4 = \frac{k_i}{4EI}. \tag{11}$$

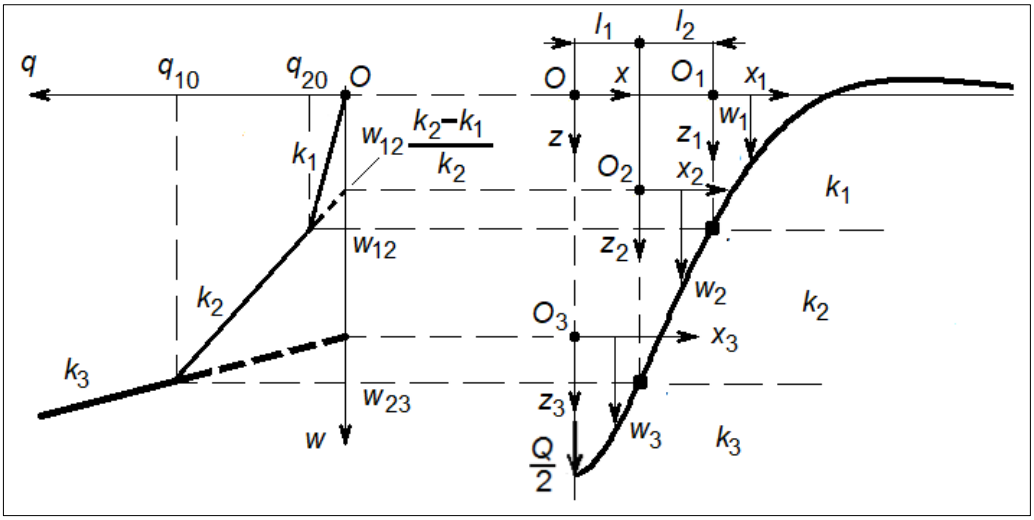

Figure 10. Scheme for calculation of the balance position of the rail under the static load

Subsequent equations can be written (for $x > 0$)

$$w(x) = \begin{cases} w_{12}\left(1-\dfrac{k_1}{k_2}\right) + u_o \dfrac{k_{11}}{k_2} + w_3(x_3) & x = x_3 \\ w_{12}\left(1-\dfrac{k_1}{k_2}\right) + w_2(x_2) & x = x_2 + l_1 \\ w_1(x_1) & x = x_1 + l_1 + l_2 \end{cases} \tag{12}$$

The boundary conditions must be fulfilled

- at $x_3 = 0$, the slope is zero and the shear force is $-Q/2$

$$\frac{dw_3(0)}{dx_3} = 0, \quad \frac{d^3 w_3(0)}{dx_3^3} = \frac{Q}{2EI} \tag{13}$$

- at $x_3 = l_1$ and $x_2 = 0$, the continuity conditions

$$w_3(l_1) = w_{23} - w_{12}\left(1-\frac{k_1}{k_2}\right) - u_o \frac{k_{11}}{k_2} \quad w_2(0) = w_{23} - w_{12}\left(1-\frac{k_1}{k_2}\right), \quad \frac{d^n w_3(l_1)}{dx_3^n} = \frac{d^n w_2(0)}{dx_2^n} \quad n = 1 \div 3. \tag{14}$$

- at $x_2 = l_2$ and x_1=0, the continuity conditions

$$w_2(l_2) = w_{12}\frac{k_1}{k_2} \quad w_1(0) = w_{12}, \quad \frac{\mathrm{d}^n w_2(l_2)}{\mathrm{d}x_2^n} = \frac{\mathrm{d}^n w_1(0)}{\mathrm{d}x_1^n} \quad n = 1 \div 3. \tag{15}$$

- for $x_1 \to \infty$, displacement vanishes

$$\lim_{x_1 \to \infty} w_1(x_1) = 0. \tag{16}$$

Rail displacement can be described by the equations

$$\begin{aligned} w_3(x_3) &= e^{-\alpha_3 x_3}\left(A_1\cos\alpha_3 x_3 + A_2\sin\alpha_3 x_3\right) + e^{\alpha_3 x_3}\left(A_3\cos\alpha_3 x_3 + A_4\sin\alpha_3 x_3\right) \\ w_2(x_2) &= e^{-\alpha_2 x_2}\left(A_5\cos\alpha_2 x_2 + A_6\sin\alpha_2 x_2\right) + e^{\alpha_2 x_2}\left(A_7\cos\alpha_2 x_2 + A_8\sin\alpha_2 x_2\right) \\ w_1(x_1) &= e^{-\alpha_1 x_1}\left(w_{12}\cos\alpha_1 x_1 + A_9\sin\alpha_1 x_1\right). \end{aligned} \tag{17}$$

Inserting Eqs. (17) in the boundary conditions, a set of 11 nonlinear equations results with the unknowns A_i, where $i = 1 \div 9$ and l_1 and l_2. Solution can be obtained using the Newton-Raphson method.

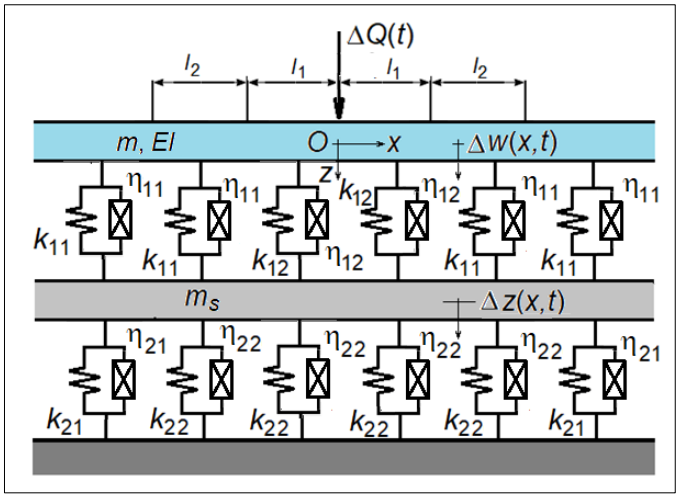

Figure 11. Track under dynamic load - linearised model with non-homogenous foundation (LMNHF)

Knowing the distances l_1 and l_2, the rail response to the dynamic component D$Q(t)$ can be calculated in terms of the receptance. To this aim, the linearised model with non-homogenous foundation of the track (LMNHF) is used (Figure 11). This model is obtained by linearizing the nonlinear model around the equilibrium position under static load by neglecting the effect of vibration around the transition sections positioned at $x = \pm l_1$ and $x = \pm (l_1 + l_2)$.

Equations of motion written for the harmonic steady-state behaviour of the w angular frequency are

$$\begin{cases} EI\dfrac{\mathrm{d}^4\Delta\bar{w}(x)}{\mathrm{d}x^4} - \omega^2 m\Delta\bar{w}(x) + \bar{k}_{12}\left[\Delta\bar{w}(x) - \Delta\bar{z}(x)\right] = 0 \\ (-\omega^2 m_t + \bar{k}_{12} + \bar{k}_{22})\Delta\bar{z}(x) - \bar{k}_{12}\Delta\bar{w}(x) = 0 \end{cases} \quad |x| < l_1$$

$$\begin{cases} EI\dfrac{\mathrm{d}^4\Delta\bar{w}(x)}{\mathrm{d}x^4} - \omega^2 m\Delta\bar{w}(x) + \bar{k}_{11}\left[\Delta\bar{w}(x) - \Delta\bar{z}(x)\right] = 0 \\ (-\omega^2 m_t + \bar{k}_{11} + \bar{k}_{22})\Delta\bar{z}(x) - \bar{k}_{11}\Delta\bar{w}(x) = 0 \end{cases} \quad l_1 \le |x| < l_1 + l_2 \tag{18}$$

$$\begin{cases} EI\dfrac{\mathrm{d}^4\Delta\bar{w}(x)}{\mathrm{d}x^4} - \omega^2 m\Delta\bar{w}(x) + \bar{k}_{12}\left[\Delta\bar{w}(x) - \Delta\bar{z}(x)\right] = 0 \\ (-\omega^2 m_t + \bar{k}_{11} + \bar{k}_{21})\Delta\bar{z}(x) - \bar{k}_{11}\Delta\bar{w}(x) = 0 \end{cases} \quad l_1 + l_2 < |x|,$$

where $\Delta\bar{w}(x)$ and $\Delta\bar{z}(x)$ are the complex amplitudes for rail and sleeper layer displacements, and $\bar{k}_{pr} = k_{pr}(1+i\eta_{pr})$ with $i^2 = -1$ and $p, r = 1, 2$.

The complex amplitude associated to the rail displacement has the following forms depending on x

$$\begin{aligned}
\Delta\bar{w}(x) &= B_1 e^{-(a_{1,3}-ia_{2,3})x} + A_2 e^{-(a_{2,3}+ia_{1,3})x} + A_3 e^{(a_{1,3}-ia_{2,3})x} + A_4 e^{(a_{2,3}+ia_{1,3})x} \quad |x| < l_1 \\
\Delta\bar{w}(x) &= A_5 e^{-(a_{1,2}-ia_{2,2})x} + A_6 e^{-(a_{2,2}+ia_{1,2})x} + A_7 e^{(a_{1,2}-ia_{2,2})x} + A_8 e^{(a_{2,2}+ia_{1,2})x} \quad l_1 \le |x| < l_1 + l_2 \\
\Delta\bar{w}(x) &= A_7 e^{-(a_{1,1}-ia_{2,1})x} + A_8 e^{-(a_{2,1}+ia_{1,1})x} \quad l_1 + l_2 < |x|,
\end{aligned} \tag{19}$$

where

$$\lambda_{1,3,n} = \pm(a_{1,n} - ia_{2,n}), \quad \lambda_{2,4,n} = \pm(a_{2,n} + ia_{1,n}) \qquad n = 1 \div 3 \tag{20}$$

are the eigenvalues of the three differential equations (18).

The complex amplitude of the rail displacement must verify the boundary conditions

- at $x = 0$, the symmetry condition and the amplitude of the shear force is $\Delta\bar{Q}$

$$\frac{\mathrm{d}\Delta\bar{w}(0)}{\mathrm{d}x} = 0, \quad \frac{\mathrm{d}^3\Delta\bar{w}(0)}{\mathrm{d}x_3^3} = \frac{\Delta\bar{Q}}{2EI} \tag{21}$$

- at $x = l_1$ and $x = l_1+l_2$, the continuity conditions

$$\frac{\mathrm{d}^n\Delta\bar{w}(l_1-0)}{\mathrm{d}x^n} = \frac{\mathrm{d}^n\Delta\bar{w}(l_1+0)}{\mathrm{d}x^n}, \quad \frac{\mathrm{d}^n\Delta\bar{w}(l_1+l_2-0)}{\mathrm{d}x^n} = \frac{\mathrm{d}^n\Delta\bar{w}(l_1+l_2+0)}{\mathrm{d}x^n} \quad n = 0 \div 3. \tag{22}$$

Inserting Eqs. (19) in the boundary conditions (21, 22), a set of 10 linear equations results with the unknowns B_i, where $i = 1 \div 10$. Solution to this system can be obtained numerically for any angular frequency ω and then, the complex amplitude of the rail emerges from Eqs. (19).

Finally, the rail receptance results

$$\bar{H}(x,\omega) = \frac{\Delta\bar{Q}}{\Delta\bar{w}(x,\omega)}. \tag{23}$$

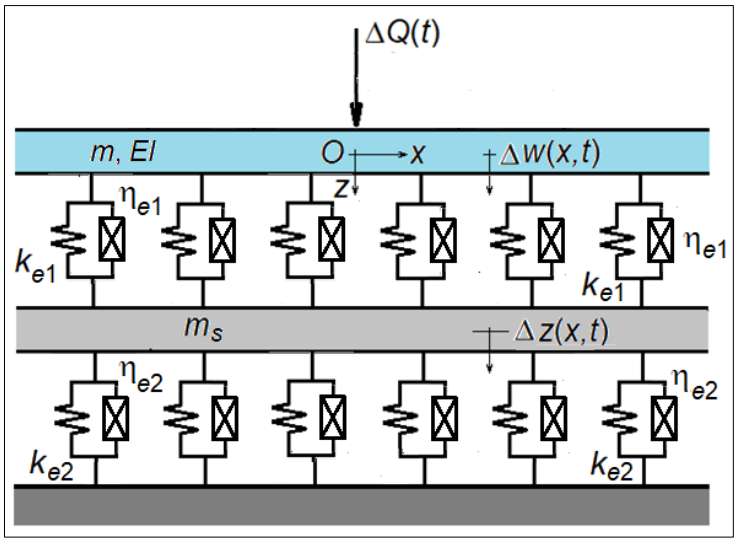

Figure 12. Linear model with homogeneous foundation (LMHF)

For comparison, an equivalent linear model with homogeneous foundation (equivalent LMHF) has been derived using the results from the rail and sleeper deflection under static load (Figure 12). The

stiffness of the two elastic layers of the model is calculated using the equations

$$k_{1e} = \frac{w_0}{w_0 - z_0} k_e, \quad k_{2e} = \frac{w_0}{z_0} k_e, \tag{24}$$

where w_0 and z_0 are the rail and sleeper deflection in acting section obtained from the nonlinear model, and k_e is the equivalent stiffness

$$k_e = \frac{k_{1e} k_{2e}}{k_{1e} + k_{2e}} = \frac{Q}{4 w_o} \sqrt[3]{\frac{Q}{w_o EI}}. \tag{25}$$

Similar, taking $k_{e1} = k_{12}$ and $k_{e2} = k_{22}$, the linear model with homogeneous foundation with 'rigid-rigid' stiffness of the two elastic layers ('rigid-rigid' LMHF) can be used as comparison.

3. Results and discussions

In this section, the track model with bilinear characteristic for the rail pad and ballast is applied to bring in light the effect of the bilinear characteristics upon the dynamic response of the rail. The parameters for the track model are presented in Table 1.

Table 1. Model parameters

Parameter	Symbol	Value	Model	
			LMNHF	LMHF
Rail linear mass	m	60 kg/m	x	x
Young's module	E	210 GPa	x	x
Moment of inertia	I	$3055 \cdot 10^{-8}$ m^4	x	x
Bending stiffness	EI	6.1455 MPa	x	x
Sleeper mass	M_t	268 kg	x	x
Sleeper bay	d	0.577 m	x	x
Sleeper linear mass (half)	m_t	232 kg/m	x	x
Rail pad stiffness	k_{11}	86.46 MN/m^2	x	x
	k_{12}	356.26 MN/m^2	x	x
	k_{1e}	151.05 MN/m^2		x
Rail pad loss factor	η_{11}	0.25	x	x
	η_{12}	0.25	x	
Ballast stiffness	k_{21}	29.79 MN/m^2	x	
	k_{22}	68.18 MN/m^2	x	
	k_{2e}	42.98 MN/m^2		x
Ballast loss factor	η_{21}	1.0	x	x
	η_{22}	1.0	x	
Static load	Q	100 kN	x	x
Distance	l_1	0.922 m	x	
	$l_1 + l_2$	0.992 m	x	

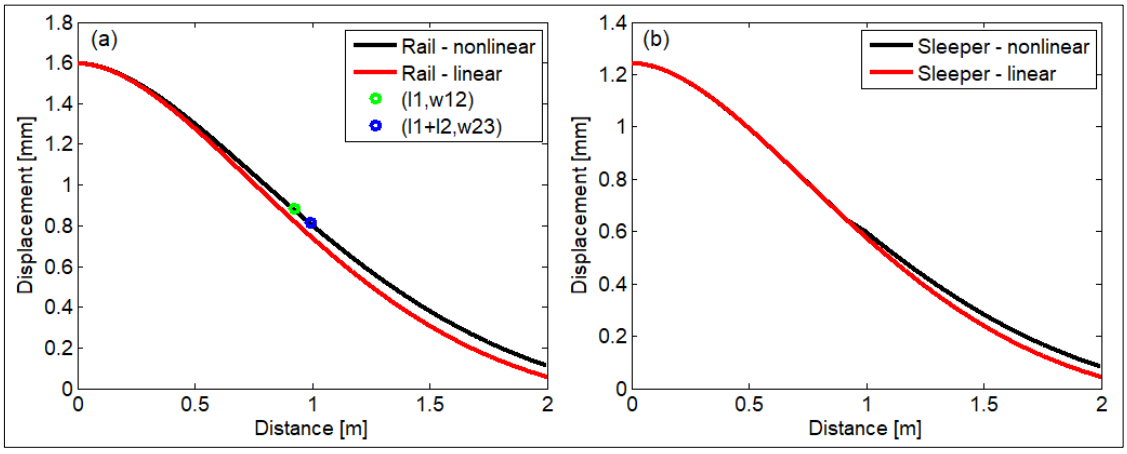

Figure 13. Track deflection under static load of 100 kN

Figure 13 shows the rail and sleepers deflection along the track due to the static load of 100 kN calculated with the nonlinear model and equivalent linear model with homogeneous foundation. First, the displacement of the rail is greater than the displacement of the sleepers, aspect which is justified by the effect of the elasticity of the rail pad. The curve showing the rail displacement calculated according to the nonlinear model shows the transition points first, in the rail pad characteristic and then, in the ballast characteristic. The results obtained with the two types of models are very close in the vicinity of the section in which the static force acts and then some differences appear. Thus, it is found that the displacement the rail and the sleepers along the track are smaller in the case of the equivalent linear model with homogeneous elastic characteristic. Consequently, it shows that this model overestimates the stiffness of the track.

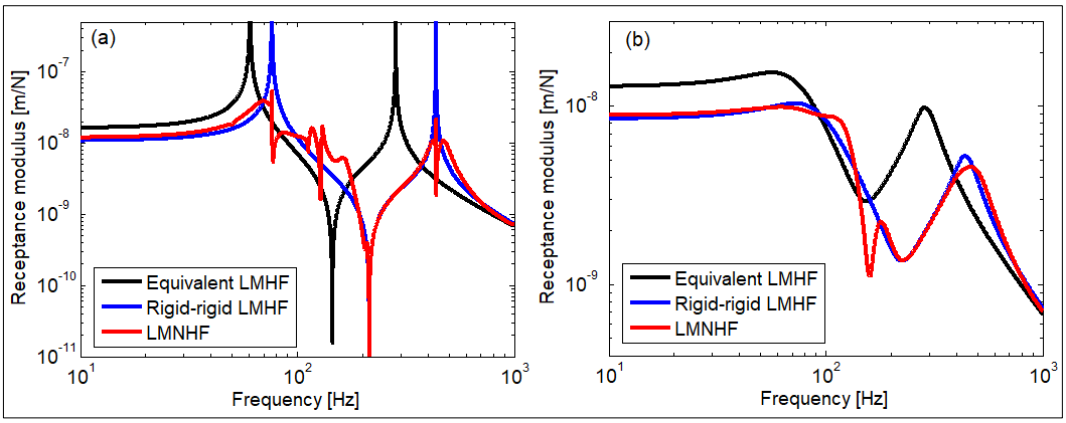

Figure 14. Rail receptance (Q = 100 kN): (a) undamped; (b) damped

Figure 14 presents the rail receptance for undamped (Figure14a) and damped (Figure 14b) cases calculated using the linearised model with non-homogeneous foundation, and with the equivalent linear model with homogeneous foundation for the static load of Q = 100 kN. Also, the rail receptance derived from 'rigid-rigid' LMHF is displayed.

Both models with homogeneous foundations exhibit two resonance frequencies and one antiresonance frequency due to the dynamic absorber effect induced by the sleepers (Figure 14 a). The two resonance frequencies are at 60.7 and 145.5 Hz for the equivalent LMHF and at 76.6 and 436.8 Hz for the 'rigid-rigid' LMHF. The antiresonance frequency is at 145.5 Hz for the equivalent LMHF and at 215.2 Hz for the 'rigid-rigid' LMHF.

The rail receptance calculated using LMNHF exhibits several peaks and dips. There is no match between the rail receptance derived from LMNHF and equivalent LMHF, excepting the high frequencies range. The explanation of former aspect lies in the fact that at high frequencies, inertial forces are prevalent and therefore the influence of elastic forces induced by the foundation (rail pad and ballast) is insignificant, and the rail receptance calculated with the two models is the same, depending on only the linear mass of the rail and frequency.

It should be noticed that the most important peaks calculated with LMNHF are at the resonance frequencies predicted by 'rigid-rigid' LMHF. Also, the main dip of the rail receptance computed using LMNHF is located at the same frequency as the antiresonance frequency of the 'rigid-rigid' LMHF. There are several similitudes between the rail receptance calculated with LMNHF and the ones calculated with 'rigid-rigid' LMHF: at low frequencies up to the first resonance frequency, between the antiresonance frequency and the second resonance frequency, and at the high frequencies. The main differences appear around the two resonance frequencies and within the range between the first resonance and the antiresonance.

The explanation for this dynamic behaviour of the rail lies in two aspects. First, it should be noted that in the vicinity of the section where the harmonic excitation force acts, both the rail pad and the ballast work on the rigid branch of the bilinear characteristic. As a result, the dynamic behaviour of the rail in

the excitation force section is strongly influenced by the rigid characteristics of the rail pad and the ballast, thus explaining the similarities above signalled. On the other hand, the change in the stiffness of the foundation due to the transition from the rigid to the elastic branch of the rail pad and ballast characteristics determines the reflected waves that change the dynamic behaviour of the rail as described.

Damping reduces the differences between the results delivered with the LMNHF and the "rigid-rigid" LMHF (Figure 14b). However, the differences signalized in the rail receptance diagram when using the equivalent LMHF remain practically unchanged.

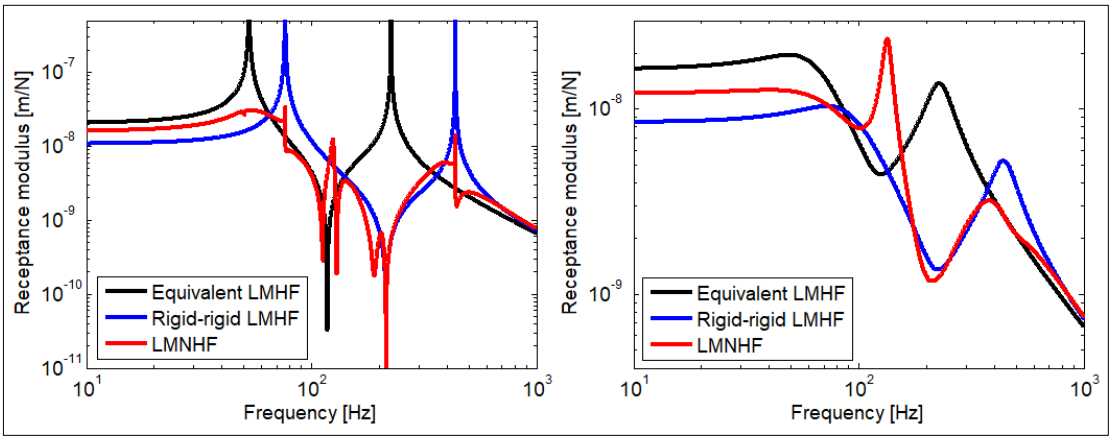

Figure 15. Rail receptance (Q = 50 kN): (a) undamped; (b) damped

Figure 15 presents the rail receptance for the static load of 50 kN calculated applying the identic methods as above and using the same loss factors for the hysteretic damping. In this case, the distances l_1 and l_2 are shorter than those calculated when Q = 100 kN, respectively, l_1 = 0.426 m and l_2 = 0.126 m. Also, the elastic layers stiffness of the equivalent LMHF differ: k_{1e} = 94.95 MN/m^2 and k_{2e} = 32.78 MN/m^2. This time, the rail receptance calculated with LMNHF is higher at low frequencies because the length of the stiff foundation is smaller, and the track becomes more flexible. There are distinct differences between the results obtained with the three models for a wideband frequency.

4. Conclusions

In this paper, a new track model incorporating the nonlinear elastic characteristics of the rubber rail pad and ballast is presented. The key features of the track model are the bilinear approximation of the nonlinear elastic characteristics and the manner in which the rail response is treated in the sense that it has two components corresponding to the static load due to the weight of the vehicle on the wheel, and the dynamic load caused by the wheel-rail interaction in the presence of unevenness.

The elastic characteristics of the rubber rail pad and ballast are described as nonlinear functions of static load depending on deflection. These nonlinear functions can be implemented in the track model using the bilinear approximation depending on the magnitude of the static load. Subsequently, the equivalent elastic characteristic of the track model is built in terms of uniform load versus rail displacement and three branches of constant stiffness each result. In this way, the track model under a static load is obtained. The nonlinear equations of equilibrium are solved using an iterative algorithm based on the Newton-Raphson method. Calculation of the rail and sleeper deflection allow to identify the position of the transition points between the branches of the equivalent elastic characteristic of the track. Further on, the track model is linearised around the equilibrium position under static load and the linearised model with nonhomogeneous foundation emerges.

Numerical application shows that the dynamic behaviour of the rail in terms of receptance depends on the static load and this dependence cannot be captured using other linear models with homogeneous foundation.

Further research is focused on the implementation of the nonlinear track model into the model of the

wheel-rail interaction to outline the influence of the elastic characteristic of the rail rubber pad on the wheel-rail vibration.

Acknowledgments: Authors express their gratitude Mr. Vasile Andrușcă, C.E.O. of the Promin Prod LTD, for the documentation regarding the rubber rail pad for K-type fastening system.

References

1.MAZILU, T., The dynamics of an infinite uniform Euler-Bernoulli beam on bilinear viscoelastic foundation under moving loads, *Procedia Engineering*, **199**, 2017, 2561-2566.
2.MAZILU, T., Interaction between moving tandem wheels and an infinite rail with periodic supports - Green's matrices of the track method in stationary reference frame, *Journal of Sound and Vibration*, **401**, 2017, 233-254.
3.ZHAI, W., WANG, K., CAI, C., Fundamentals of vehicle-track coupled dynamics, *Vehicle System Dynamics*, **47**(11), 2009, 1349–1376.
4.ZHANG, X., THOMPSON, D.J., SQUICCIARINI, G., Sound radiation from railway sleepers, *Journal of Sound and Vibration* **369**, 2016, 178-194.
5.CHENG, G., HE, Y., HAN, J., SHENG, X., THOMPSON, D., An investigation into the effect of modelling assumptions on sound power radiated from a high-speed train wheelset, *Journal of Sound and Vibration* **495**, 2021, 115910.
6.MORTENSEN, J. FAURHOLT, J. F., HOVAD, E., WALTHER, J., H., Discrete element modelling of track ballast capturing the true shape of ballast stones, *Powder Technology* **386**, 2021, 144-153.
7.KAEWUNRUEN, S., REMENNIKOV, A. M., Sensitivity analysis of free vibration characteristics of an in-situ railway concrete sleeper to variations of rail pad parameters, *Journal of Sound and Vibration* **298**, 2006, 453-461.
8.SAINZ-AJA, J. A., ISIDRO A. CARRASCALA, I. A., DIEGO FERREÑOA, D., POMBO, J., JOSE A. CASADO, J. A., DIEGO, S., Influence of the operational conditions on static and dynamic stiffness of rail pads, *Mechanics of Materials* **148**, 2020, 103505.
9.CHERKASOV, V., YURKIN, Y., AVDONIN, V., SUNTSOV, D., Self-adhesion X-ray Shielding Composite Material of EPDM Rubber with Barite: Mechanical Properties, *Mater. Plast.*, **57**(1), 2020, 28-36.
10.KISS, I., BACIU, A. M., BORDEASU, I., MICU, L. M., Compressive Strength of Stripes and Flakes of Recycled Polyethylene Terephthalate (PET) Added Concrete, *Mater. Plast.*, **57**(1), 2020, 244-252.
11.XU, L., NIU, L., Effect of Polypropylene Fiber on Frost Resistance of Cemented Soil, *Mater. Plast.* **57(2)** 2020, 78-86.
12.VOICU, A. D., HADAR, A., VLASCEANU, D., TUDOSE, D. I., Vibrational Study of a Helicopter Tail Rotor Blade with Different Polymer Inner Core Materials, *Mater. Plast.*, **57**(2), 2020, 169-178.
13.LIU, B., MIRJALILI, M., VALIPOUR, P., PORZAL, S., NOURBAKHSH, S., Morphology and Mechanical Properties of Polyethylene Terephthalate/Ethylene Propylene Diene Monomer (PET/ EPDM) in the Presence of Nanoclay, *Mater. Plast.*, **57**(3), 2020, 249-259.
14.RAMADAN, I., TANASE, M., Experimental Study Regarding the Influence of Welding Parameters on the Mechanical Behavior of High Density Polyethylene Pipes, *Mater. Plast.*, **57**(4), 2020, 209-215.
15.WU, T.X., THOMPSON, D. J., The Effects of Local Preload on the Foundation Stiffness and Vertical Vibration of Railway Track, *Journal of Sound and Vibration* **219**, 1999, 881–904.
16.REMENNIKOV, A. M., KAEWUNRUEN, S., Determination of dynamic properties of rail pads using an instrumented hammer impact technique, *Acoustics Australia* 33, 2005, 63-67.
17. REMENNIKOV, A. M., KAEWUNRUEN, S., Laboratory measurements of dynamic properties of rail pads under incremental preload, 19th Australasian Conference on the Mechanics of Structures and Materials, Nov 29 - Dec 1 2007, Christchurch, New Zealand, Taylor & Francis, 319-324.
18. OREGUI, M., LI, Z., DOLLEVOET, R. An investigation into the modeling of railway fastening, *International Journal of Mechanical Sciences* **92**, 2015, 1-11.

19. GE, X., LING, L., YUAN, X., WANG, K., Effect of distributed support of rail pad on vertical vehicle-track interactions, *Construction and Building Materials* **262**, 2020, 120607.
20. ZHU, S., CAI, C., SPANOS P. D., A nonlinear and fractional derivative viscoelastic model for rail pads in the dynamic analysis of coupled vehicle–slab track systems, *Journal of Sound and Vibration* **335**, 2015, 304-320.
21. OREGUI, M., LI, Z., DOLLEVOET, R. An investigation into the vertical dynamics of tracks with monoblock sleepers with a 3D finite-element model, *Proc IMechE Part F: J Rail and Rapid Transit* 2015 https://doi.org/10.1177/0954409715569558.
22. LUO, Y., LIU, Y., YIN, H.P., Numerical investigation of nonlinear properties of a rubber absorber in rail fastening systems, *International Journal of Mechanical Sciences* **69**, 2013, 107-113.
23.*** Technical specification rail rubber pad for K-type rail fastening system, ST 02/2011, T.C. PROMIN PROD L.T.D.

Manuscript received: 29.06.2021